Microporous and Mesoporous Materials 295 (2020) 109907

Contents lists available at ScienceDirect

Microporous and Mesoporous Materials

journal homepage: http://www.elsevier.com/locate/micromeso

# Shaping of MOFs via freeze-casting method with hydrophilic polymers and their effect on textural properties

Emrah Hastürk, Simon-Patrick Höfert, Burhan Topalli, Carsten Schlüsener, Christoph Janiak *

*Institut für Anorganische Chemie und Strukturchemie, Heinrich-Heine-Universität, D-40204, Düsseldorf, Germany*

ARTICLE INFO

*Keywords:*
Metal-organic frameworks
MOFs
Shaping
Monolith
Hydrophilic shift
Freeze-casting

ABSTRACT

Shaping of metal-organic frameworks (MOFs) and tuning of their sorption properties is a very important and challenging aspect for the usage of MOFs for many applications. Both shaping and tuning can be addressed by composite preparation as an effective method. Herein, we present the shaping of the hydrothermally stable MOFs aluminum fumarate, MIL-160(Al) and MIL-101(Cr) using the freeze-casting method with the hydrophilic polymer binders polyacrylic acid (PAA), sodium polyacrylate (PAANa), polyethylene glycol (PEG), polyethylene imine (PEI), polyvinyl alcohol (PVA) and polyvinyl pyrrolidone (PVP). Furthermore, the effect of in-situ cross-linking below the freezing point (cryopolymerization) on the textural properties of monoliths was also investigated using MIL-101(Cr) and aluminum fumarate with the polymer PVA. The selected MOFs were chosen due to their outstanding stability, sorption properties and differing hydrophilicities. In the obtained mechanically stable monoliths, each MOF showed a different compatibility with the used polymers. From 21 different MOF@polymer composites with 80 wt% loading of MOF, 12 of them exhibited negligible pore blocking effects and very high nitrogen sorption properties in correspondence with the MOF mass fraction. On the other hand, water uptake is especially in cases of MOF@PVA and MOF@PVP in good agreement with the MOF fraction and can be enhanced by the contribution of the hydrophilic polymer to the composite. In particular, most MIL-101(Cr) composites showed a hydrophilic shift to lower relative pressure $p \cdot p_0^{-1}$ compared to the rather hydrophobic neat MIL-101 (Cr). IR spectroscopy indicated a clear interaction of PEI with the Al-MOFs aluminum fumarate and MIL-160 (Al) resulting in MOF pore blocking. The molecular weight of the polymer is not significant for the freeze-casting method but plays an important role in the cryopolymerization.

## 1. Introduction

Metal-organic frameworks (MOFs) are hybrid materials, composed of metal atoms and organic linkers, possessing potential voids [1]. The high variety of metal atoms and linkers enabled, so far, more than 70 000 different MOF structures (until 2017 [2]) which were investigated for potential applications in catalysis [3,4], gas storage and gas separation [5–7], cyclic adsorption applications [8–10], etc. Among these applications, the investigation of MOFs in cyclic adsorptions chillers (ACs) and thermally driven heat pumps (TDHPs) gained considerable attention in the last decade [11,12]. ACs and TDHPs are an eco-friendly and promising technology in the field of low-electricity energy utilization [13]. The choice of adsorbent materials in the ACs and TDHPs requires, inter alia, hydrothermal stability, appropriate water sorption properties with respect to the relative pressure region, high water uptake capacity and proper operating adsorption-desorption conditions [11].

Water is the adsorbate of choice for heat transformation applications and the water adsorption-desorption behavior of the relevant adsorbents, which also includes MOFs, is very essential. Related applications based on the water adsorption-desorption of MOFs are also dehumidification [14] and water harvesting from air [15]. The most relevant MOFs for water sorption-based applications are given in the literature [11]. Among these we selected aluminum fumarate (Alfum) [16], MIL-160(Al) [17] and MIL-101(Cr) [18] for their proven hydrothermal stability and high water uptake capacity, albeit in different relative pressure regions, corresponding to different hydrophilicities. For MIL-160(Al) the steep rise of the *S*-shaped isotherm lies within $0.03 < p \cdot p_0^{-1} < 0.15$, while the steep rise for Alfum occurs within $0.2 < p \cdot p_0^{-1} < 0.3$ [19,20]. MIL-101(Cr) which reaches above 1 g $g^{-1}$ of water vapor uptake requires the relative pressure range of $0.4 < p \cdot p_0^{-1} < 0.6$. More information about the sorption properties of the MOFs can be found in the Supp. Info. Thus, the order of decreasing hydrophilicity is MIL-160

* Corresponding author.
*E-mail address:* janiak@uni-duesseldorf.de (C. Janiak).

https://doi.org/10.1016/j.micromeso.2019.109907
Received 12 October 2019; Received in revised form 13 November 2019; Accepted 18 November 2019
Available online 20 November 2019

(Al) > Alfum ≫ MIL-101(Cr). Clearly, the interesting rise of the *S*-shaped water sorption isotherm of MIL-101(Cr) [21] lies outside of the desired relative pressure range of about $0.1 < p{\cdot}p_0^{-1} < 0.3$ [22]. Still, its high water loading and large pores have led to various chemical modifications of MIL-101(Cr) either by functionalizing the terephthalate (BDC) linker [23–25] or grafting of hydrophilic groups to the metal center [26] in order to achieve a more hydrophilic MIL-101(Cr) [27], which would make this modified MIL-101(Cr) a suitable candidate for water sorption-based applications.

Additionally, one of the important requirements for most applications of MOFs is the usage of a shaped body instead of the neat-MOF powder materials. In most cases, MOFs are obtained as a microcrystalline powder material from their synthesis. Powder materials have disadvantages in handling, such as dusting and low bulk density due to the small particle size [28]. While MOFs need to be shaped for applications, at the same time shaping needs to preserve the initial porous properties of MOFs [29–31]. Shaping procedures of MOFs have been recently reviewed pointing out pelletizing, granulating, coating and monolith formation as preferred methods [32,33].

In many shaping methods, the use of a binder material is needed [32] which could cause pore-blocking of the MOF [29–31]. Because of that, each MOF must be tested and judiciously selected for a particular shaping procedure and binder and vice-versa [34,35]. In this work, we used the fabrication of MOF-polymer monoliths by the so-called freeze-casting method (ice-templating). The freezing process generates ice crystals which are removed by freeze-drying to give a stable ice-templated macroporous material [36]. A monolith has the advantages of robustness, easy handling and high density [37,38].

Application of the freeze-casting method in MOF formulation and in MOF chemistry, at large, is rare. To the best of our knowledge freeze-casting was applied to dry MOFs [39] and in the shaping of HKUST-1 to obtain hierarchically porous monoliths directly after synthesis without using any binder [37]. Additionally, a UiO-66@chitosan monolith was prepared using the freeze-casting method [40]. The UiO-66@chitosan monolith was used for the wastewater treatment and showed a high adsorption capacity of methylchlorophenoxypropionic acid (MCPP) with 34 mg $g^{-1}$ close to the MCPP adsorption of neat UiO-66 with 36 mg $g^{-1}$. However, the UiO-66@chitosan monolith composite had lost most of the apparent BET surface area, S(BET). The apparent S(BET) dropped from 1034 $m^2$ $g^{-1}$ for neat UiO-66 to 339 $m^2$ $g^{-1}$ in the UiO-66@chitosan composite which contained nearly 99 wt% UiO-66 [40]. Another example is the preparation of an ultralight hierarchically porous monolith, which was prepared by the high internal phase emulsion (HIPE) technique, combining UiO-66 and polyvinyl alcohol (PVA), followed by freeze-drying [41].

A related method to freeze-casting is cryopolymerization in which macroporous monoliths are obtained via a polymerization reaction with a cross-linker under the freezing point of the solvent, generally water [42]. This in-situ cross-linking below the freezing point is also used to obtain stable monoliths. However, this method requires a cross-linker, such as glutaraldehyde, glycerol diglycidyl ether, [43,44].

The polymers polyacrylic acid (PAA), sodium polyacrylate (PAANa), polyethylene glycol (PEG), polyethylene imine (PEI), polyvinyl alcohol (PVA) and polyvinyl pyrrolidone (PVP) were selected for their known hydrophilicity (see Fig. S7 in Supp. Info. for the polymer repeat unit). At $p{\cdot}p_0^{-1} = 0.9$ the amount of adsorbed water is 440 mg $g^{-1}$ for polyacrylic acid, 920 mg $g^{-1}$ for sodium polyacrylate, 50 mg $g^{-1}$ for polyethylene glycol, 860 mg $g^{-1}$ for polyethylene imine, 185 and 210 mg $g^{-1}$ for polyvinyl alcohol with different hydrolysis degrees and 560 mg $g^{-1}$ for polyvinyl pyrrolidone. These polymers are commercially available in bulk quantities at a relatively low price.

For the selection of MOF and polymer, it is important to consider which type of application the composite is used for. For instance, MOFs should meet some criteria for use in AHT, such as hydrothermal stability and high water uptake capacity with the *S*-shaped isotherm lies in the relative pressure range of about $0.01 < p{\cdot}p_0^{-1} < 0.3$. The choice of polymer is also important to ensure that the polymer does not compromise the desired sorption properties of the MOF and even possibly improves the sorption properties. In the example below, PEI was chosen because of its known $CO_2$ adsorption properties, which provided enhanced $CO_2$ sorption properties in MOF@PEI composite [45].

Composite materials should show similar or even enhanced material properties compared to the individual components and their weight percent. For example, a composite based on glass fibers with PEI and epoxy resin (EP) retained the water vapor uptake for PEI of around 800 mg $g^{-1}$ [46]. MIL-101(Cr)@R,F-xeorgel with 77 wt% of MIL-101(Cr) has the maximum water uptake of 0.88 g $g^{-1}$, which matches the expected value with 0.84 g $g^{-1}$ [30]. In composite materials, it is even possible to surpass the initial properties of the neat component. A MIL-101(Cr)@PEI composite with 50 wt% of MIL-101(Cr) adsorbs at 1 bar nearly 5 mmol $(CO_2){\cdot}g^{-1}$ (of composite), which is three times more $CO_2$ adsorption than MIL-101(Cr) alone [45].

In this contribution, we report 21 MOF@polymer monoliths composed of the MOFs Alfum, MIL-160(Al) or MIL-101(Cr) with the polymers PAA, PAANa, PEG, PEI, PVA (two different hydrolysis degrees) and PVP using the freeze-casting method. In addition, in-situ cross-linking below the freezing point (cryopolymerization) was performed using the MOFs Alfum and MIL-101(Cr) and the polymer PVA.

## 2. Experimental section

### 2.1. Materials and methods

All used chemicals were commercially obtained from various sources and used without further purification: Aluminum fumarate (Basolite™ A520, BASF, abbreviated in this work as Alfum), chromium (III) nitrate nonahydrate ($Cr(NO_3)_3{\cdot}9H_2O$, Acros Organics, 99%), nitric acid (Grüssing, 65 wt%), 1,4-benzenedicarboxylic acid ($H_2BDC$, Acros Organics, >99%), N,N′-dimethylformamide (DMF, VWR, p. a.), tetramethylammonium hydroxide (Alfa Aesar, 25 wt% in $H_2O$), basic aluminum diacetate ($Al(OH)(CH_3COO)_2$, VWR), glutaraldehyde (Alfa Aesar, 25 wt % in $H_2O$), ethanolamine (Chimia, 99%), hydrochloric acid (Fisher Scientific, ≥ 37%), 2,5-furandicarboxylic acid (Sigma-Aldrich, >97%), ethanol (VWR, p. a.), polyacrylic acid with an average $M_w$ of 100 kDa (Sigma-Aldrich, 35 wt% in $H_2O$, abbreviated as PAA), sodium polyacrylate with an average $M_w$ of 15 kDa (Sigma-Aldrich, 35 wt% in $H_2O$, abbreviated as PAANa), polyethylene glycol with an average $M_w$ of 12 kDa (Sigma-Aldrich, abbreviated as PEG), branched polyethylene imine with an average $M_w$ of 70 kDa (Alfa Aesar, 30 wt% in $H_2O$, abbreviated as PEI), polyvinyl alcohol with an average $M_w$ of 125 kDa and 98% hydrolyzed (Sigma-Aldrich, Mowiol® 20–98, abbreviated as PVA(98)), polyvinyl alcohol with an average $M_w$ of 10–26 kDa and 86–89% hydrolyzed (abbreviated as PVA(88)1), polyvinyl alcohol with an average $M_w$ of 31 kDa and 88% hydrolyzed (Sigma-Aldrich, Mowiol® 4–88, abbreviated as PVA(88)2), polyvinyl alcohol with an average $M_w$ of 67 kDa and 88% hydrolyzed (Sigma-Aldrich, Mowiol® 8–88, abbreviated as PVA(88)3), polyvinyl alcohol with an average $M_w$ of 130 kDa and 88% hydrolyzed (Sigma-Aldrich, Mowiol® 18–88, abbreviated as PVA (88)4), polyvinyl alcohol with an average $M_w$ of 205 kDa and 88% hydrolyzed (Sigma-Aldrich, Mowiol® 40–88, abbreviated as PVA(88)5) and polyvinyl pyrrolidone with an average $M_w$ of 360 kDa (Sigma-Aldrich, abbreviated as PVP).

Powder X-ray diffractograms (PXRD) were obtained at ambient temperature on a Bruker D2 Phaser (300 W, 30 kV, 10 mA) using Cu-Kα radiation (λ = 1.54 182 Å) between $5° < 2\theta < 50°$ with a scanning rate of 0.15° $s^{-1}$ for Alfum, MIL-160(Al) and related composites and between $5° < 2\theta < 35°$ with a scanning rate of 0.0275° $s^{-1}$ for MIL-101(Cr) and related composites. The diffractograms were obtained on a flat "low background sample holder", in which at low angle the beam spot is strongly broadened so that only a fraction of the reflected radiation reaches the detector, hence the low relative intensities measured at 2θ <

7°. The analyses of the diffractograms were carried out with the "Match 3.11" software.

Nitrogen physisorption measurements of MIL-160(Al), Alfum and related composites were carried out on a Nova 4000e from Quantachrome. Nitrogen physisorption isotherms of polymers, MIL-101(Cr) as well as MIL-101(Cr)@polymer composites were carried out on an Autosorb-6 from Quantachrome at 77 K. Argon physisorption isotherms were carried out on a Quantachrome Autosorb iQ MP at 87 K, which was set by a Cryocooler temperature controller from Qantachrome. Water physisorption measurements of MOFs and polymer composites were measured volumetrically on a VSTAR from Quantachrome at 293 K with the following equilibrium settings: Equilibrium points number: 10; Equilibrium points Interval time of 120 s for $0.001 \leq p{\cdot}p_0^{-1} \leq 0.400$, 180 s 0.450 for $\leq p{\cdot}p_0^{-1} \leq 0.900$ during adsorption and 90 s for $0.800 \leq p{\cdot}p_0^{-1} \leq 0.600$, 120 s for $0.500 \leq p{\cdot}p_0^{-1} \leq 0.010$ during desorption. Before each sorption measurement, all probes were activated under vacuum ($<2 \times 10^{-2}$ mbar) at 373 K for 3 h. An exception were neat PEG monoliths, which were activated at 333 K for 3 h because of the low melting point of 65 °C for PEG. "Brunauer-Emmett-Teller (BET) surface areas (designated as 'apparent S(BET)' for microporous materials [47]) were calculated from the nitrogen physisorption isotherms using the described conditions given in the publication by Rouquerol et al. [48].

Scanning electron microscopy (SEM) images were taken by a Jeol JSM-6510LV QSEM advanced electron microscope with a $LaB_6$ cathode at 5–20 keV. The microscope was equipped with a Bruker Xflash 410 silicon drift detector for energy-dispersive X-ray spectrometry (EDX).

FT-Infrared (IR) spectra were measured in ATR-mode (Platinum ATR-QL, diamond crystal) on a Bruker TENSOR 37 IR spectrometer in the range of 4000−550 $cm^{-1}$.

## 2.2. Synthesis

### 2.2.1. Synthesis of MIL-101(Cr) with $HNO_3$

MIL-101(Cr) was synthesized hydrothermally according to the literature (large scale synthesis route) [49]. $Cr(NO_3)_3{\cdot}9H_2O$ (4.8 g, 12.0 mmol), 1,4-benzenedicarboxylic acid (2.03 g, 12.2 mmol), $HNO_3$ (0.54 mL, 12.0 mmol, 65 wt%) and deionized $H_2O$ (60 mL) were placed in a 90 mL Teflon-liner and stirred for 2 h. The Teflon-liner was inserted in a steel autoclave and heated to 200 °C within 8 h, held at this temperature for 15 h and then cooled down in 24 h to room temperature (rt). The precipitated green powder was centrifuged and washed consecutively with DMF (125 mL for 1 h and 125 mL for 20 h) and later on with EtOH (125 mL for 1 h). Before each solvent change, the sample was separated by centrifugation. After the final centrifugation, the green crystalline powder was dried under vacuum. Yield 2.24 g, 78% based on the "activated" product formula $Cr_3(\mu_3\text{-}O)(OH)(H_2O)_2(BDC)_3$, $C_{24}H_{17}Cr_3O_{16}$, 717.37 g $mol^{-1}$. This MIL-101(Cr) was used for the monolith preparation via the freeze-casting method.

### 2.2.2. Synthesis of MIL-101(Cr) with TMAOH

According to the literature [50] 1,4-benzenedicarboxylic acid (1.98 g, 11.9 mmol), tetramethylammonium hydroxide (TMAOH, 25 wt% in $H_2O$) (1.08 mL, 3.00 mmol) and deionized $H_2O$ (60 mL) were placed in a 90 mL Teflon-liner and stirred for 4 h, then $Cr(NO_3)_3{\cdot}9H_2O$ (4.82 g, 12.0 mmol) was added to the solution and stirred further for 1 h. The Teflon-liner was inserted in a steel autoclave and heated to 180 °C within 12 h, held at this temperature for 48 h and then cooled down in 18 h to rt. The green powder was centrifuged and washed consecutively with the following order: deionized water (100 mL at rt), DMF (300 mL at 115 °C for 40 h), EtOH (2 × 150 mL at rt), EtOH (200 mL under reflux for 24 h), EtOH (200 mL under reflux for 72 h). Before each solvent change, the cooled-down suspension was centrifuged and the supernatant was removed. After final centrifugation, the green crystalline powder was dried under vacuum to give 2.40 g of a powdery product (84% for $Cr_3(\mu_3\text{-}O)(OH)(H_2O)_2(BDC)_3$, $C_{24}H_{17}Cr_3O_{16}$, 717.37 g $mol^{-1}$). MIL-101(Cr) obtained under basic conditions was used for the monolith preparation involving in-situ PVA cross-linking.

### 2.2.3. Synthesis of MIL-160(Al)

The synthesis of MIL-160(Al) was carried out by a modified method of Serre et al. [19] $Al(OH)(CH_3COO)_2$ (3.9 g, 24 mmol) and 2,5-furandicarboxylic acid (4.1 g, 26 mmol) were dispersed in a 100 mL round bottom flask in deionized water (25 mL) and refluxed at 115 °C for 24 h. The resulting white solid was recovered by subsequent centrifugation and was washed two times with 100 mL EtOH at rt (ca. 1 h and overnight). After centrifugation and vacuum drying overnight at 100 °C a yield of 4.53 g (95% based on the framework formula [$Al(OH)(O_2C\text{–}C_4H_2O\text{–}CO_2)$], $C_6O_6H_3Al$, 198.07 g $mol^{-1}$) was collected. MIL-160(Al) was obtained as a white solid.

The MOFs were stored under ambient conditions under moist air. Due to their microporosity and hydrophilicity water is adsorbed into the MOFs upon storage. Directly before composite formation the MOFs were activated by drying for 3 h at 100 °C under dynamic vacuum ($2\text{-}5{\cdot}10^{-2}$ mbar).

### 2.2.4. Fabrication of MOF@polymer monoliths and polymer monoliths

All monoliths were prepared using a prime protocol. In the following, the preparation of 80 wt% composites is generally described for all prepared monoliths.

The amount of 60 mg polymer was dissolved in 1 mL of $H_2O$, if necessary (e.g. PVA) by heating to over 80 °C. After complete dissolution, the polymer solution was added to 240 mg of activated MOF and stirred for 3 h with 1000 rpm. Afterwards the suspension was filled in a disposable 1 mL syringe. Beforehand the cannula side of the syringe had been cut open (see Fig. S4 in Supp. Info.).

The filled syringe was frozen in liquid nitrogen for approximately 5 min. After freezing, the syringe was allowed to warm, until the solidified monolith content could be pressed from the syringe and placed in a liquid nitrogen cooled test tube. The test tube, which was then immediately placed under dynamic vacuum ($1 \times 10^{-3}$ mbar) for 24 h to remove the water, giving the MOF@polymer monolith. A schematic fabrication procedure of the composite monoliths is shown in Section 3.3.

The neat polymer monoliths were prepared in the same way without the addition of MOF.

The obtained monoliths are described as MOF*xx*@polymer where *xx* refers to the wt% of MOF in the composite. For example, MIL-101(Cr) 80@PAA has 80 wt% loading of MIL-101(Cr) in the monolith with the PAA polymer. wt% was calculated according to (x mg MOF)/(x mg MOFs + x mg polymer) × 100%.

### 2.2.5. Fabrication of MOF@polymer monoliths and polymer monoliths with in-situ cross-linking of PVA by cryopolymerization

MOF@polymer cryogel monoliths were synthesized according to a method modified from the literature [51]. The polymer solutions were prepared as mentioned in Section 2.2.4 (dissolving 100 mg polymer in 2 mL of water). To this solution, finely powdered MOF was added (50 mg for 33 wt% loading and 100 mg for 50 wt% loading) and stirred vigorously for 1 h.

Two drops of HCl (5 mol $L^{-1}$) were added to this suspension which was subsequently cooled in an ice-bath. After addition of glutaraldehyde (80 μL, 10 g $L^{-1}$ final solution) at 0 °C, the viscose suspension was placed in a 5 mL cylindrical glass and kept in the freezer at −20 °C for 19 h. After thawing to rt (30 min), the glass was broken and the obtained monolith was washed by agitation in deionized water (24 h), in ethanolamine solution to block possible free aldehyde groups (0.4 mol $L^{-1}$ in water; 1 h) and subsequently in deionized water (24 h).

The monoliths with PVA(98), PVA(88)2 and PVA(88)3 were dried by freeze-drying. MIL-101(Cr)@CP-PVA(98) and Alfum@CP-PVA(98) samples were obtained as green and white stable monoliths, respectively. The MIL-101(Cr) used here had been synthesized under basic conditions (Section 2.2.2). Composites with cross-linked

(cryopolymerized) PVA were designated with "CP" in front of the polymer in the sample name, e.g., as MIL-101(Cr)50@CP-PVA(98) for 50 wt% MIL-101(Cr) loaded in cross-linked PVA(98).

The neat polymer monoliths CP-PVA(88)2 and CP-PVA(88)3 were prepared in the same way without the addition of MOF.

CP-PVA(98) monoliths were prepared in the same way without the addition of MOF and after addition of ethanolamine solution and deionized water, the monolith was dehydrated in ethanol for 72 h, exchanging the solvent every 24 h. Finally, the white product was dried via super critical $CO_2$.

## 3. Results and discussion

### 3.1. Preparation of the MOFs

In this study, two different synthesis methods were used for the preparation of MIL-101(Cr). For the preparation of MIL-101(Cr)@polymer monoliths via the freeze-casting method, MIL-101(Cr) was synthesized with the addition of $HNO_3$ instead of problematic HF [49]. The measured apparent S(BET) of 3170 $m^2\ g^{-1}$ is in good agreement with the literature values for this method between 3100 and 3500 $m^2\ g^{-1}$ [49]. More structural details on MIL-101(Cr) are given in the Supp. Info., Section S3, PXRD in Fig. S9 and SEM images in Fig. S16.

MIL-101(Cr) synthesized with the base tetramethylammonium hydroxide (TMAOH) was obtained with an apparent BET surface area of 2425 $m^2\ g^{-1}$ (see Fig. 8 for nitrogen sorption isotherm), somewhat lower than the literature value (3197 $m^2\ g^{-1}$) [50]. The PXRD results (see Fig. S22 in Supp. Info.) are in good agreement with the simulated diffractogram of MIL-101(Cr). For the SEM-images of MIL-101(Cr) from this route, see Fig. 7. MIL-101(Cr) obtained with TMAOH was used in the monolith preparation by in-situ PVA cross-linking.

MIL-160(Al) was synthesized using 2,5-furandicarboxylic acid and basic aluminum diacetate [17]. MIL-160(Al) was obtained with an apparent BET surface area of 1100 $m^2\ g^{-1}$ comparable to the reported value with an apparent BET surface area of 1070 $m^2\ g^{-1}$ [17] (see Fig. 4 for the nitrogen sorption isotherm). More information on the MIL-160(Al) structure can be found in the Supp. Info., Section S2; PXRD in Fig. S9.

Alfum was obtained as a commercial product, which exhibited an apparent BET surface area of around 950 $m^2\ g^{-1}$ (see Fig. 4 for nitrogen sorption isotherm) [52]. More information about the Alfum structure is given in the Supp. Info., Section S1, PXRD in Fig. S9.

The porosity properties of Alfum, MIL-160(Al) and MIL-101(Cr) are summarized in Table 5 and for MIL-101(Cr) synthesized with TMAOH in Table S4 in the Supp. Info.

### 3.2. Preparation of the polymer monoliths via freeze-casting method

The prepared polymer solution with a mass fraction of 5.7 wt% (this concentration was also used for the preparation of the MOF@polymer monolith) was placed in a syringe, which was cut open from the cannula side, and afterwards submerged in liquid nitrogen for 5 min. The monolith preparation with PAA, PVP, PVA(98), PVA(88), PEG and PAANa was possible, however strong shrinkage during drying caused deformation of their initial cylindrical shapes (see Fig. S5 in Supp. Info.). The strong shrinkage can be explained due to the very low polymer concentration. Furthermore, PVA monoliths were mechanically more stable in comparison to other polymer monoliths. PEI is liquid at room temperature; therefore it was not possible to obtain PEI as a monolith. Therefore, nitrogen sorption analysis of PEI was not performed but water sorption was done after activation of the liquid PEI at 373 K. According to the nitrogen sorption data, the derived BET surface areas of polymer monoliths are below 30 $m^2\ g^{-1}$. The water sorption isotherms of the polymer monoliths or liquid PEI can be categorized as Type III [47] and indicate relatively high water vapor adsorption, especially for PEI and PAANa, in the late relative pressure range of around 0.9 (Fig. 1).

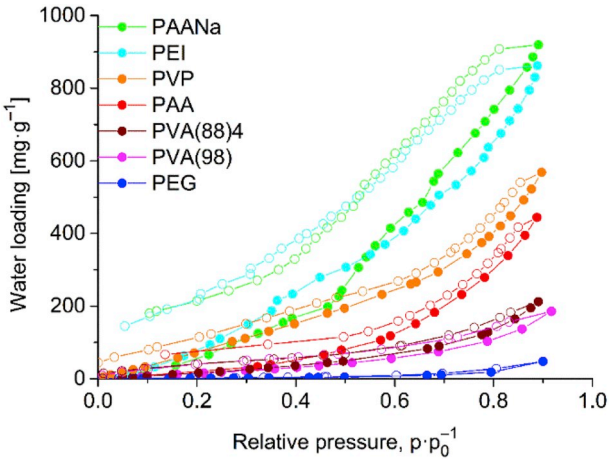


**Fig. 1.** Water vapor adsorption-desorption isotherms of PAA, PAANa, PEG, PVA(98), PVA(88)4 and PVP monoliths as well as liquid PEI measured at 293 K. Adsorption is depicted with filled, desorption with empty symbols.

**Table 1**
Water vapor uptake of polymer monoliths and liquid PEI (at different relative pressures).

| Polymers | Water uptake [mg $g^{-1}$] at $p \cdot p_0^{-1}$ = | | | | | | |
|---|---|---|---|---|---|---|---|
| | 0.15 | 0.20 | 0.30 | 0.35 | 0.40 | 0.60 | 0.90 |
| PAA | 15 | 23 | 31 | 39 | 53 | 123 | 444 |
| PAANa | 37 | 67 | 112 | 140 | 171 | 414 | 919 |
| PEG | 1 | 2 | 2 | 3 | 3 | 7 | 48 |
| PEI | 51 | 79 | 150 | 187 | 238 | 390 | 862 |
| PVA(98) | 11 | 14 | 22 | 27 | 31 | 56 | 185 |
| PVA(88)4 | 12 | 16 | 25 | 31 | 36 | 70 | 212 |
| PVP | 54 | 73 | 112 | 132 | 152 | 225 | 568 |

The maximum adsorbed water vapor amount of around 900 mg $g^{-1}$ was observed here for PAANa monoliths, followed by 860 mg $g^{-1}$ for liquid PEI, both at the relative pressure of 0.9 and in agreement with the literature [46,53]. In Table 1 the amount of water uptake for all polymer monoliths and liquid PEI is compared at different relative pressure ranges. From the uptake values the order of hydrophilicity of the polymer binders would be PAANa ≈ PEI > PVP > PAA > PVA ≫ PEG. PAANa monoliths and liquid PEI are the best performing materials in almost each given range of the relative vapor pressure. Remarkable is the very large hysteresis of liquid PEI and PAANa monoliths, which can be explained by relatively strong hydrogen-bonding interactions of either the amino- (PEI) or carboxylate groups (PAANa) with the water molecules.

The measured water uptake of the PEG monolith at $p \cdot p_0^{-1} = 0.9$ reached only 50 mg $g^{-1}$ (determined twice to exclude measurement error) and is contrary to the reported uptake of 600 mg $g^{-1}$ [54].

A PAA monolith gave nearly 450 mg $g^{-1}$ water uptake at 20 °C and at $p \cdot p_0^{-1} = 0.9$ which is slightly higher than the literature value of 350 mg

**Table 2**
Comparison of different preparation methods regarding the accessible surface area and monolith-shape retention.[a]

| Methods | LNFD | LNAD[b] | F18FD | F18AD |
|---|---|---|---|---|
| S(BET) [$m^2\ g^{-1}$] | 621 ± 11[a] | – | 596 ± 6[a] | 599 ± 10[a] |
| Shape retention | successful | complete deformation | successful | partial deformation |

[a] Based on the preparation of an Alfum80@PVA(88)4 monolith. Average value of 6 measurements (three times from top and three times from bottom pieces of the monolith).

[b] Because of unsuccessful shaping, the sample was not analyzed further (see Fig. S6 in Supp. Info.).

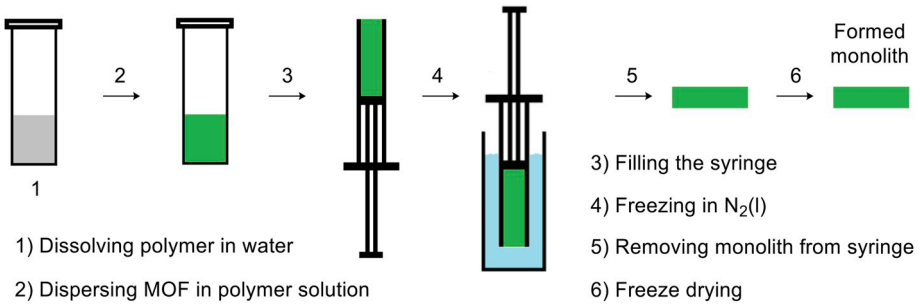


**Fig. 2.** Preparation of the MOF@polymer monolith via freeze-casting method.

$g^{-1}$ at 30 °C [55]. The water sorption isotherms of PVA and PVP monoliths are comparable with the literature [56,57].

### 3.3. Preparation of the MOF@polymer monoliths via freeze-casting method

The freeze-casting method was tested under different freezing and drying conditions, using the Alfum80@PVA (88)4 monoliths. Freezing of the composites was either carried out in liquid nitrogen (−193 °C for 5 min) or in a freezer (−18 °C for 24 h) with subsequent drying in air or under freeze-drying conditions. Therefore, four different preparation methods are possible, which can be abbreviated as LNFD (freezing in $N_2$ (liq) and freeze-drying), LNAD (freezing in $N_2$ (liq) and air drying), F18FD (freezing in freezer at −18 °C and freeze-drying) and F18AD (freezing in freezer at −18 °C and air drying). Reproducibility of each method was tested three times by evaluating the obtained composite shape and surface area. Each method indicates with very low standard deviation a good reproducibility for the apparent S(BET) (see Table 2). As MOF Alfum was used for this evaluation due to good pore accessibility, simple synthesis under mild conditions and its inexpensive starting materials. Alfum was also commercially available as Basolite™ A520 from BASF. PVA was selected as binder material because of a low price, larger variability of molecular weight and good mechanical stability. The MOF content was prepared up to 80 wt% in the monolith. Because of the high viscosity of the obtained suspension with 80 wt% of MOF in the MOF/polymer suspension, a higher loading amount of the MOF was not tried. Another reason is that some MOF@polymer monoliths were fragile already with 80 wt% of MOF.

Based on the superior results in shaping and slightly higher apparent S(BET), LNFD was chosen as the standard method for the preparation of the MOF@polymer composites. A schematic fabrication procedure of the composite monoliths is shown in Fig. 2.

It was possible with LNFD and F18FD to preserve the shape of the monolith. Interestingly, air drying was only partially successful for F18AD, in the case of LNAD complete deformation was observed (see Fig. S6). The thawing and necessary longer drying time for air-drying (AD) clearly is the cause of deformation.

Volume-based sorption properties instead of the more typical specific or mass-based uptake amounts are important for the usage of MOF in restricted volumes. Because of that reason, we compare the bulk density and tapped density of the neat MOFs with the density of the monoliths (see Table S2 and Table S3 in Supp. Info.). The bulk density and tapped density are explained in Supp. Info. Section S12. MIL-101(Cr) showed the smallest bulk and tapped density with 0.08 and 0.29 g $cm^{-3}$, respectively. On the other hand, MIL-160(Al) has the highest bulk and tapped density among the investigated MOFs with a value of 0.25 and 0.59 g $cm^{-3}$, respectively. In comparison to the neat MOFs, only the MOF@polymer composite monoliths obtained by air drying (F18AD, with partial deformation of the shape) achieved densities of up to 0.44 g $cm^{-3}$, which were in the same range as the tapped density of neat Alfum (0.46 g $cm^{-3}$). Whereas the freeze-drying provided monoliths with lower densities in the range of 0.30 and 0.39 g $cm^{-3}$ for the Alfum80@polymer monoliths and 0.28 and 0.41 g $cm^{-3}$ for the MIL-160 (Al)80@polymer monoliths.

### 3.4. Effect of molecular weight of the polymer on the monoliths

The effect of the molecular weight of the polymer on the freeze-casting method was studied by using the different PVA(88) polymers with varying molecular weight of 10–26 kDa (PVA(88)1), 31 kDa (PVA (88)2), 67 kDa (PVA(88)3), 130 kDa (PVA(88)4) and 205 kDa (PVA(88) 5) and by comparing monoliths with 80 wt% of Alfum MOF loading. There is a small tendency that the surface area and pore volume, that is, the pore accessibility increases with increasing molecular weight of the polymer (Table 3), which can be explained by less pore penetration or pore blocking in the case of less flexible longer chains. While the pore accessibility of PVA(88)1, PVA(88)2 and PVA(88)3 is around 70% (judged by % of calc. S(BET)), the pore accessibility can be enhanced up to 86% by using higher molecular weight PVA(88)5.

### 3.5. Effect of MOF amount on the monoliths

The effect of increased MOF content on monoliths was also exemplarily analyzed using PVA(88) and Alfum. Different Alfum contents varying from 30 wt% to 80 wt% were prepared in the 5.7 wt% polymer solution. The porosity properties of the resulting monoliths are listed in Table 4. As expected, with increasing Alfum amount rises also its still accessible surface area and pore volume in the monolith. The best results were achieved with 80 wt% of Alfum (the highest MOF percentage in this work) in the composite, having an apparent BET surface area of 612 $m^2 g^{-1}$ and pore volume of 0.319 $cm^3 g^{-1}$, which correspond 80% and 82% of calculated values, respectively. The increasing percentage of pore accessibility with increasing Alfum amount can be explained by the lower polymer fraction leading to less polymer chains or chain ends available for pore blocking phenomena. Conversely, an increasing PVA (88) to Alfum ratio leads to the formation of thicker PVA(88) layers surrounding the Alfum particles with pore blocking.

### 3.6. Powder X-ray diffraction patterns of the monoliths

The retained crystallinity of the MOFs in the prepared monoliths was ascertained with PXRD. In all MOF80@polymer composites (Alfum80@polymers, MIL-160(Al)80@polymers and MIL-101(Cr) 80@polymers), the main reflexes were retained unchanged, indicating the preserved crystallinity of the MOFs upon composite formation (see Fig. 3).

### 3.7. IR spectra of the monoliths

In general, the IR spectra of the MOF@poylmer composite were an overlay of the spectra of the pure polymer and the MOF. Even if for composites with 80 wt% MOF and 20 wt% polymer, the corresponding IR absorption bands of the polymer are very weak and, in some cases, not observable. However, with increasing polymer amount the bands

**Table 3**
Porosity properties of Alfum80@PVA monoliths with different molecular weights of the polymer.

| Sample[a] | $M_w$ (PVA) [kg mol$^{-1}$] | $S$(BET)[b] exp. [m$^2$ g$^{-1}$] (% of S(BET) calc.) | $S$(BET) calc.[c] [m$^2$ g$^{-1}$] | $V$(pore)[d] [cm$^3$ g$^{-1}$] (% of $V$(pore) calc.) | $V$(pore) calc.[c] [cm$^3$ g$^{-1}$] |
|---|---|---|---|---|---|
| Alfum | | 946 | – | 0.478 | – |
| Alfum80@PVA(88)1 | 10–26 | 542 (72) | 757 | 0.308 (80) | 0.386 |
| Alfum80@PVA(88)2 | 31 | 522 (69) | 757 | 0.295 (77) | 0.385 |
| Alfum80@PVA(88)3 | 67 | 546 (72) | 757 | 0.301 (78) | 0.386 |
| Alfum80@PVA(88)4 | 130 | 612 (80) | 761 | 0.319 (82) | 0.388 |
| Alfum80@PVA(88)5 | 205 | 651 (86) | 759 | 0.347 (90) | 0.385 |

[a] Prepared by liquid nitrogen freeze-drying (LNFD).
[b] Apparent S(BET) values were determined from $N_2$ sorption isotherms at 77 K with a standard deviation ± 20 m$^2$ g$^{-1}$ (thereby apparent S(BET) values were calculated from the nitrogen physisorption isotherms using the described conditions in the publication by Rouquerol et al. [48] with at least 3 points. Due to the high variation of about a few hundred m$^2$ g$^{-1}$, the S(BET) of MIL-101(Cr) and corresponding composites were determined over 7 points in the relative pressure range between 0.05 and 0.2).
[c] Calculated apparent S(BET) and calculated micro- and small mesopore volume $V$(pore) in the monoliths were determined as the sum of the mass-weighted S(BET) or V(pore) of the MOFs and the respective polymer (PAA, PAANa, PEG, PEI, PVA(98), PVA(88) or PVP) monolith from the following formula (Ia) or (Ib), respectively:

$$\mathrm{S(BET)calc.} = \frac{\mathrm{wt\%\ of\ polymer}}{100} \times \mathrm{S(BET,polymer)} + \frac{\mathrm{wt\%\ of\ MOF}}{100} \times \mathrm{S(BET,MOF)} \quad (\mathrm{Ia})$$

with apparent $S$(BET): Alfum = 946 m$^2$ g$^{-1}$; MIL-160(Al) = 1134 m$^2$ g$^{-1}$; MIL-101(Cr) = 3171 m$^2$ g$^{-1}$; Surface area of polymers are PAA = 5 m$^2$ g$^{-1}$; PAANa = 4 m$^2$ g$^{-1}$; PEG = 5 m$^2$ g$^{-1}$; PEI = 0 m$^2$ g$^{-1}$; PVA(98) = 26 m$^2$ g$^{-1}$; PVA(88)1 = 0 m$^2$ g$^{-1}$; PVA(88)2 = 0 m$^2$ g$^{-1}$; PVA(88)3 = 0 m$^2$ g$^{-1}$; PVA(88)4 = 19 m$^2$ g$^{-1}$; PVA(88)5 = 12 m$^2$ g$^{-1}$; PVP = 17 m$^2$ g$^{-1}$;

$$\mathrm{V(pore)calc.} = \frac{\mathrm{wt\%\ of\ polymer}}{100} \times \mathrm{V(pore,polymer)} + \frac{\mathrm{wt\%\ of\ MOF}}{100} \times \mathrm{V(pore,MOF)} \quad (\mathrm{Ib})$$

with $V$(pore): Alfum = 0.478 cm$^3$ g$^{-1}$; MIL-160(Al) = 0.445 cm$^3$ g$^{-1}$; MIL-101 = 1.348 cm$^3$ g$^{-1}$; PAA = 0.0135 cm$^3$ g$^{-1}$; PAANa = 0.005 cm$^3$ g$^{-1}$; PEG = 0.004 cm$^3$ g$^{-1}$; PEI = 0 cm$^3$ g$^{-1}$; PVA(98) = 0.042 cm$^3$ g$^{-1}$; PVA(88)1 = 0.018 cm$^3$ g$^{-1}$; PVA(88)2 = 0.012 cm$^3$ g$^{-1}$; PVA(88)3 = 0.016 cm$^3$ g$^{-1}$; PVA(88)4 = 0.024 cm$^3$ g$^{-1}$; PVA(88)5 = 0.011 cm$^3$ g$^{-1}$; PVP = 0.015 cm$^3$ g$^{-1}$. The values and equations are also used for Tables 4 and 5.
[d] Total pore volumes V(pore) were determined from $N_2$ sorption isotherms at 77 K ($p{\cdot}p_0^{-1} = 0.90$) for pores ≤ 20 nm.

**Table 4**
Porosity properties of Alfum@PVA monoliths with different Alfum content.

| Sample[a] | $S$(BET)[b] exp. [m$^2$ g$^{-1}$] (% of calc. $S$(BET)) | $S$(BET) calc.[c] [m$^2$ g$^{-1}$] | $V$(pore)[d] [cm$^3$ g$^{-1}$] (% of calc. $V$(pore)) | $V$(pore) calc.[c] [cm$^3$ g$^{-1}$] |
|---|---|---|---|---|
| Alfum | 946 | - | 0.482 | – |
| Alfum30@PVA(88)4 | 145 (49) | 297 | 0.110 (69) | 0.161 |
| Alfum43@PVA(88)4 | 215 (51) | 418 | 0.139 (63) | 0.220 |
| Alfum45@PVA(88)4 | 223 (51) | 436 | 0.149 (65) | 0.229 |
| Alfum60@PVA(88)4 | 353 (61) | 575 | 0.209 (70) | 0.297 |
| Alfum69@PVA(88)4 | 453 (69) | 659 | 0.244 (72) | 0.338 |
| Alfum75@PVA(88)4 | 490 (69) | 714 | 0.268 (73) | 0.365 |
| Alfum78@PVA(88)4 | 533 (72) | 742 | 0.281 (74) | 0.378 |
| Alfum80@PVA(88)4 | 612 (80) | 761 | 0.319 (82) | 0.388 |

[a] Prepared by liquid nitrogen freeze-drying (LNFD).
[b,c,d] See Table 3 for the footnote explanations.

will clearly be seen in the IR spectra (Fig. S10a).

The IR spectra of the Alfum80@PEI composites show the disappearance of the PEI band at ~1300 cm$^{-1}$ (Fig. S12a in Supp. Info). In the spectra of MIL-160(Al)80@PEI this band either also disappears or is shifted to about 1346 cm$^{-1}$ (Fig. S12b in Supp. Info). This disappearance of the 1300 cm$^{-1}$ band is also seen in the composite prepared upon mixing of $AlCl_3{\cdot}6H_2O$ with a 5.7 wt% aqueous PEI solution and freeze dried (see Fig. S13 in Supp. Info. for the IR spectra). In the literature the disappearance of this band occurs concomitant with protonation of PEI [58] and hydration of PEI [59] with the latter probably also being accompanied by proton transfer from water. Hydrated $Al^{3+}$ metal atoms act as strong Brønsted acids through the polarization of the coordinated aqua ligands which lowers the p$K_a$ value of $H_2O$ from 14 to about 5 (in $[Al(H_2O)_6]^{3+}$) [60].

### 3.8. Nitrogen sorption of the monoliths

Nitrogen sorption studies for the determination of BET surface area and porosity show significant effects of the polymer on the pore accessibility of the MOF in the obtained monoliths (Fig. 4, Table 5).

Among the Alfum80 and MIL-160(Al)80@polymer composites the ones with PVA(98) revealed the best porosity results in absolute values and also with the highest percentage of the calculated mass-weighted $S$(BET) or $V$(pore), followed by PVA(88)4 and PVP. At the same time the Alfum80@polymer and MIL-160(Al)80@polymer composites with PEI were lowest in pore accessibility, followed by PEG, due to the high pore blocking effects, which for PEI were discussed with the IR spectra.

To further elucidate the pore blocking, we also measured $H_2$ sorption of MIL-160@PEI. $H_2$ has a kinetic diameter of 0.29 nm, compared to $N_2$ with 0.36 nm [61]. The $H_2$ sorption (see Fig. S20 in Supp. Info.) showed similar tendency as in the case of $N_2$ sorption. So, the unexpected water sorption can be explained due to interaction of water with amine group of the polymers as swelling of the PEI.

MIL-101(Cr) exhibits the expected nitrogen adsorption isotherm of Type 1b [47] with the characteristic step for MIL-101 before $p{\cdot}p_0^{-1} = 0.2$ indicating microporous windows and mesoporous pores [18]. The shape of the nitrogen adsorption isotherms remains as Type 1b also in the composites although the amount of adsorbed nitrogen differs with the polymer (see Fig. 4c). The MIL-101(Cr)@PVP monolith shows the best results for the composite materials with an apparent S(BET) of 2470 m$^2$ g$^{-1}$ and pore volume of 1.120 cm$^3$ g$^{-1}$, which indicates no pore blocking effect. Yet, with MIL-101(Cr) all polymers, except for PEI showed comparable apparent S(BET) in the range of 2100 and 2500 m$^2$ g$^{-1}$ and pore volumes of 0.9 and 1.1 cm$^3$ g$^{-1}$ with retention of accessible porosity of over 85% compared to the mass-weighted MIL content. In earlier work, we already noted that pore blocking effects in polymer

**Table 5**
Results of nitrogen sorption measurements for MOFs and MOF@polymer composites.

| Sample[a] | | *S*(BET)[b] exp. [$m^2g^{-1}$] (% of calc. *S*(BET)) | *S*(BET) calc.[c] [$m^2\ g^{-1}$] | *V*(pore)[d] [$cm^3\ g^{-1}$] (% of calc. *V*(pore)) | *V*(pore) calc.[c] [$cm^3\ g^{-1}$] |
|---|---|---|---|---|---|
| Alfum | | 946 | – | 0.478 | – |
| **Alfum** | 80@PAA | 340 (45) | 758 | 0.245 (64) | 0.385 |
| | 80@PAANa | 477 (63) | 758 | 0.257 (67) | 0.384 |
| | 80@PEG | 182 (24) | 758 | 0.198 (52) | 0.384 |
| | 80@PEI | 149 (20) | 757 | 0.111 (29) | 0.383 |
| | 80@PVA(98) | 658 (86) | 762 | 0.348 (89) | 0.391 |
| | 80@PVA(88)4 | 612 (80) | 761 | 0.319 (82) | 0.388 |
| | 80@PVP | 584 (77) | 760 | 0.321 (83) | 0.386 |
| MIL-160(Al) | | 1134 | – | 0.445 | - |
| **MIL-160(Al)** | 80@PAA | 808 (89) | 908 | 0.340 (95) | 0.359 |
| | 80@PAANa | 417 (46) | 908 | 0.214 (60) | 0.357 |
| | 80@PEG | 285 (31) | 908 | 0.142 (40) | 0.357 |
| | 80@PEI | 43 (5) | 907 | 0.035 (10) | 0.356 |
| | 80@PVA(98) | 925 (101) | 912 | 0.382 (105) | 0.364 |
| | 80@PVA(88)4 | 800 (88) | 911 | 0.357 (99) | 0.361 |
| | 80@PVP | 802 (88) | 911 | 0.343 (96) | 0.359 |
| MIL-101(Cr) | | 3171 | – | 1.348 | - |
| **MIL-101(Cr)** | 80@PAA | 2203 (87) | 2538 | 1.007 (93) | 1.081 |
| | 80@PAANa | 2152 (85) | 2538 | 0.974 (90) | 1.079 |
| | 80@PEG | 2234 (88) | 2538 | 1.056 (98) | 1.079 |
| | 80@PEI | 1199 (47) | 2537 | 0.562 (52) | 1.078 |
| | 80@PVA(98) | 2251 (89) | 2542 | 1.048 (96) | 1.087 |
| | 80@PVA(88)4 | 2225 (88) | 2541 | 1.032 (95) | 1.083 |
| | 80@PVP | 2470 (97) | 2540 | 1.120 (104) | 1.081 |

[a]Prepared by liquid nitrogen freeze-drying (LNFD).
[b,c,d] See Table 3 for the footnote explanations.

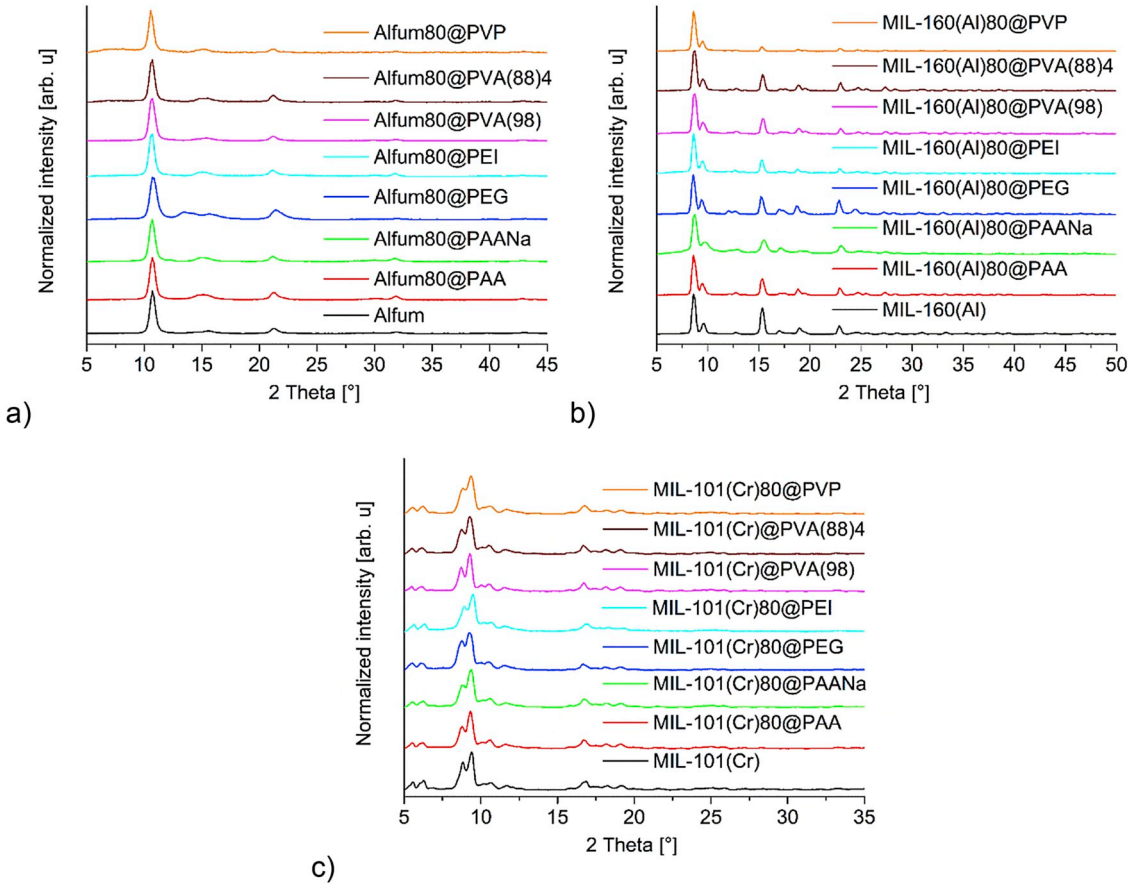


**Fig. 3.** Experimental powder X-ray diffraction pattern of (a) Alfum and Alfum@polymer monoliths, (b) MIL-160(Al) and MIL-160(Al)@polymer monoliths as well as (c) MIL-101(Cr) and MIL-101(Cr)80@polymer monoliths.

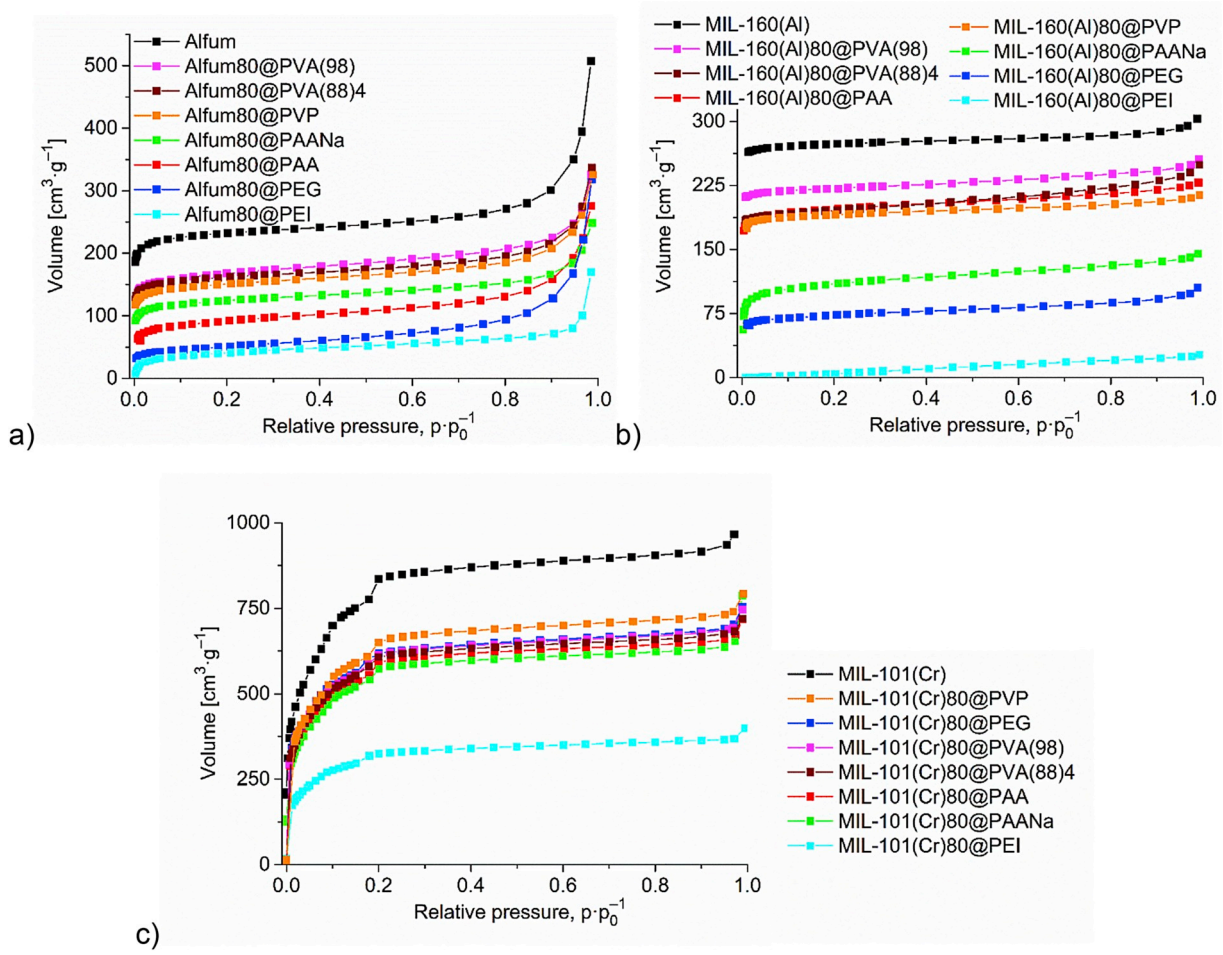


**Fig. 4.** Nitrogen adsorption isotherms of (a) Alfum and Alfum80@polymer monoliths (b) MIL-160(Al) and MIL-160(Al)80@polymer monoliths as well as (c) MIL-101(Cr) and MIL-101(Cr)80@polymer monoliths. (For clarity, only the adsorption isotherms are shown.)

composites of MIL-101(Cr) with its large pore windows were always lowest when compared to other MOFs with smaller pore openings in MOF@polymer composites [29–31]. The stronger interaction of MIL-101(Cr) with PEI, which was discussed in the IR part, is obviously the reason for the reduction of the apparent S(BET) and pore volume in MIL-101(Cr)80@PEI monolith.

Generally, the reduction of the BET surface area and pore volume of the MOF@polymer composite is explained by blocking of the pores or pore mouths with the polymer chain ends. Enveloping of the MOF particles by polymer sheaths, acting as a thin film will also reduce accessibility to the MOF pores, even if the pore mouths remain open. Importantly and different from earlier work on MIL-100 and MIL-101 compounds [29–31], the freeze-casting method allows also to achieve little pore blockage for MOFs of lower porosity such as Alfum and MIL-160 with selected polymers.

Only PEI and PEG showed very low pore accessibility for the Alfum and MIL-160 monoliths. Both polymers have low melting points compared to the other polymers. PEI used in this work has a melting

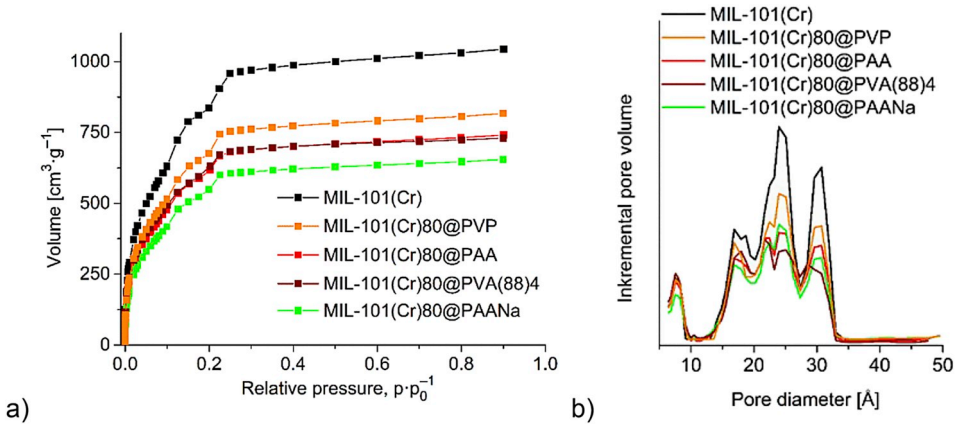


**Fig. 5.** (a) Argon adsorption isotherm of MIL-101(Cr) and MIL-101(Cr)80@PVP, -PAA, -PVA(88)4 and -PAANa at 87 K and (b) corresponding pore size distribution calculated with the DFT kernel "Ar at 87 K zeolites/silica" (spher./cylinder. pores, NLDFT equ.). (For clarity, only the adsorption isotherms are shown.)

point below rt, while PEG melts at 65 °C. For this reason, the activation temperature during degassing was also lowered from 100 °C to 60 °C for MOF@PEI and MOF@PEG composites. However, the reduction of the activation temperature led to similar sorption properties and pore accessibility (see Fig. S18 in Supp. Info.).

For the exemplary micropore size and distribution analysis, we carried out argon sorption measurements, which are more reliable than nitrogen sorption measurement for the micropore analysis. As suggested in the literature we used for the DFT analysis the DFT kernels Ar at 87K zeolites/silica (spherical/cylindrical pores, NLDFT equilibrium) [62]. In Fig. 5 the argon sorption isotherms and pore size distribution of MIL-101 (Cr) and MIL-101(Cr)80@polymers can be seen. The pore size distribution curve of bulk MIL-101(Cr) represents, with small deviation, the pore sizes, which are expected from the crystal structure analysis of MIL-101(Cr) (see Fig. S3). The pore with 7.9 Å can be related to the micropore in super tetrahedron (8.6 Å) (see Fig. 5) and the distribution

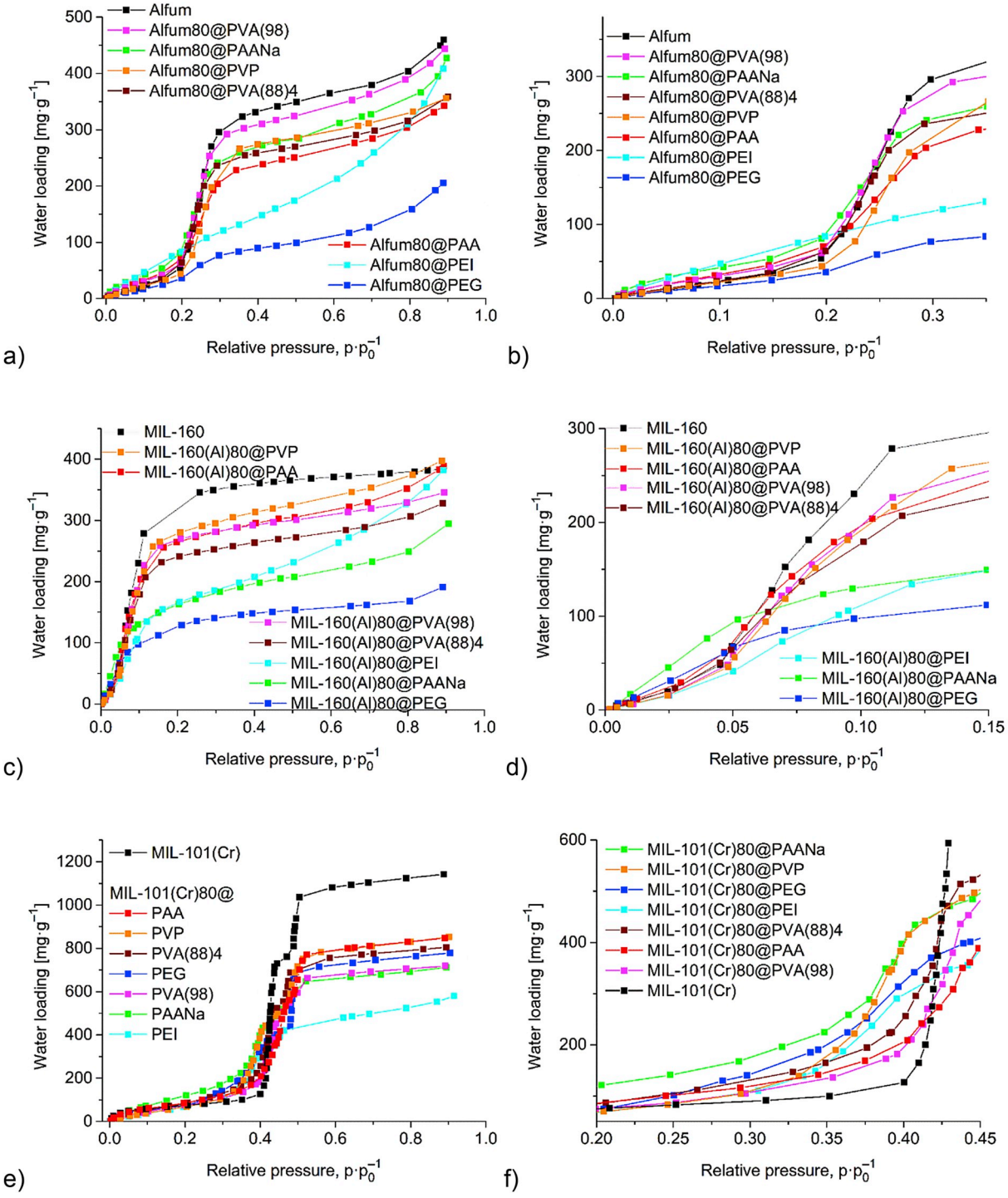


**Fig. 6.** Water vapor sorption isotherm of (a) Alfum and Alfum80@polymer monoliths (c) MIL-160(Al) and MIL-160(Al)80@polymer monoliths (e) MIL-101(Cr) and MIL-101(Cr)80@polymer monoliths as well as corresponding lift of samples in the relevant relative pressure range for (b) Alfum and Alfum80@polymer monoliths (d) MIL-160(Al) and MIL-160(Al)80@polymer monoliths (f) MIL-101(Cr) and MIL-101(Cr)80@polymer monoliths. (For clarity, only the adsorption isotherms are shown.)

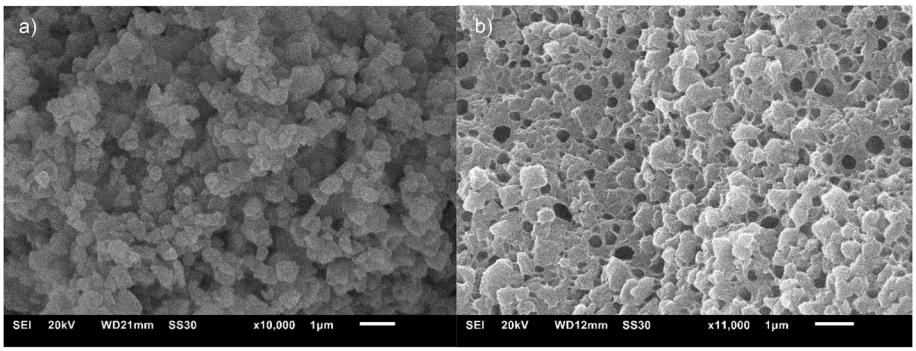


**Fig. 7.** Scanning electron microscopy (SEM) images of the (a) MIL-101(Cr) synthesized with TMAOH and (b) MIL-101(Cr)45@CP-PVA(88)3

in the range from 13 to 33 Å can be assigned to the pore windows of MIL-101(Cr) with 12, 14 and 16 Å as well as to the mesoporous cages with 29 and 34 Å [18]. The rather identical pore size distribution for MIL-101(Cr) and its composites suggests that there is no extra interfacial volume, that is, no MOF-polymer interface volume (so-called void volume) has formed [63]. In Fig. 5b it can be seen that primarily the pore volume due to the larger pores between 20 and 35 Å diameter is reduced. The polymer chains more easily penetrate these larger pores.

### 3.9. Water sorption of the monoliths

The *S*-shape of the water sorption isotherms of the MOF@polymer monoliths remains similar to the isotherms of the neat MOF (Fig. 6). Also, at first sight, the specific water uptake of the MOF@polymer monoliths has decreased, when compared to the neat MOFs, as could be expected from the "only" 80 wt% MOF content in the monoliths (Fig. 6a, c,e, columns in Table 6 at $p{\cdot}p_0^{-1} = 0.9$). However, a closer view reveals a significant increase in water uptake for the monolith over the neat MOF in the lower relative pressure region which is shown enlarged in Fig. 6b, d,f. The assignment of lower relative pressure region depends on the respective MOF and is defined as the region before the steep uptake in the *S*-shaped adsorption isotherm. For Alfum the lower relative pressure region was set to $p{\cdot}p_0^{-1} \leq 0.15$, for MIL-160(Al) to $p{\cdot}p_0^{-1} \leq 0.05$ and for MIL-101(Cr) to $p{\cdot}p_0^{-1} \leq 0.4$. The water uptake at these values is listed in the grey shaded column in Table 6 together with the expected calculated water loading based on the mass-weighted uptake of the MOF and polymer at this relative pressure (as % and absolute value). It is evident that the experimental water uptake in the lower relative pressure region can surpass the calculated value by a large amount. For example, for Alfum80@PEI the measured water uptake at $p{\cdot}p_0^{-1} = 0.15$ is at 176% of the calculated value followed by Alfum80@PAANa with 160%. For MIL-160(Al)@PAANa the experimental water uptake is at 165% at $p{\cdot}p_0^{-1} = 0.05$, next to MIL-160(Al)@PAANa with 133%. Finally, for MIL-101(Cr) @PEG the water uptake is at 330% at $p{\cdot}p_0^{-1} = 0.40$, followed by MIL-101(Cr)@PVP with 310% MIL-101(Cr)@PAANa with 305%. Evidently for all MIL-101(Cr)@polymer monoliths at $p{\cdot}p_0^{-1} = 0.40$ the measured water uptake is at least almost double (>190%) then from what was calculated. That is, for MIL-101(Cr) the beginning of the steep increase *S*-shaped water sorption isotherm has been significantly shifted to a lower relative pressure in the monolith composites, even with the least hydrophilic PEG binder. This hydrophilic shift is comparable with the effect of the amino group in $NH_2$-MIL-101(Cr) compared to non-functionalized MIL-101(Cr) in the relative pressure range up to 0.4 [24].

Yet, when the whole adsorption isotherm is considered especially the PEI composites and in part also the PAANa composites do not keep up their early water uptake which appears to be clearly dominated by the polymer alone. At higher relative pressure, that is, after the steep *S*-increase, the water uptake of the PEI composites follows more the curvature of the pure polymer, best seen for Alfum80@PEI, with little contribution from the 80 wt% MOF content. This can be correlated to the $N_2$ uptake, BET surface area and porosity, which was consistently the lowest for the MOF@PEI composites (Table 5), hence, PEI led to MOF pore blocking. For MIL-160(Al)@PEI this pore blocking was also confirmed by $H_2$ sorption (see above and Fig. S20 in Supp. Info.). We note that the kinetic diameter of $H_2$ with 0.29 nm [61] is comparable to the kinetic diameter of $H_2O$ (0.27 nm) [64].

In order to understand the exact adsorption mechanism of water sorption in each composite, it would be necessary to perform high level of theoretical calculations [65,66]. However, some general aspects can already be deduced which are important for the water sorption properties, such as the hydrophobicity/hydrophilicity of the ligand, pore size, defects (missing linkers and missing clusters), open-metal site of clusters and hydrogen-bonding capabilities of functional linker groups [67]. With respect to the above effects, changes in pore size and the

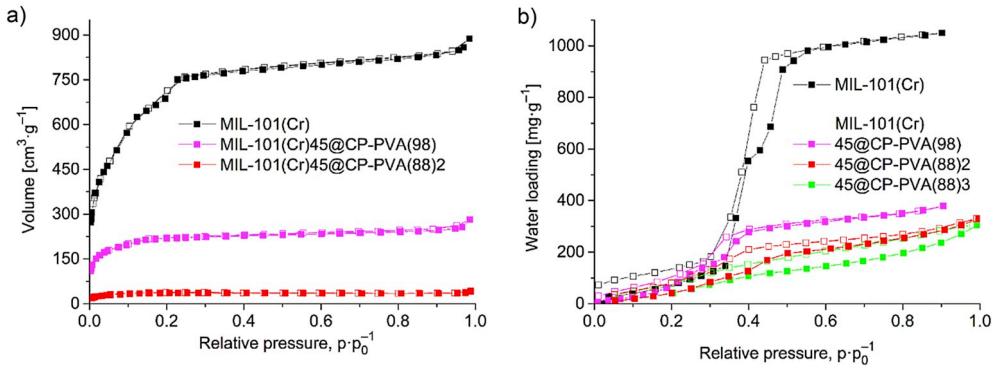


**Fig. 8.** (a) Water vapor adsorption-desorption isotherms of MIL-101(Cr)45@CP-PVA(98), MIL-101(Cr)45@CP-PVA(88)2, MIL-101(Cr)45@CP-PVA(88)3 and MIL-101(Cr) synthesized with TMAOH (b) nitrogen adsorption-desorption isotherms of MIL-101(Cr)45@CP-PVA(98), MIL-101(Cr)45@CP-PVA(88)2 and MIL-101(Cr) synthesized with TMAOH. Adsorption is depicted with filled, desorption with empty symbols.

**Table 6**
Results of water vapor sorption measurements.

| | Sample[a] | Exp. water load [mg·g⁻¹] | (% of calc. loading) | {calc. water load [b]} [mg·g⁻¹] |
|---|---|---|---|---|
| | | at | | |
| | | $p \cdot p_0^{-1}$ = 0.15 | $p \cdot p_0^{-1}$ = 0.35 | $p \cdot p_0^{-1}$ = 0.90 |
| | Alfum | 34 (-) {-} | 321 (-) {-} | 460 (-) {-} |
| Alfum | 80@PAA | 47 (154) {30} | 229 (87) {264} | 347 (76) {457} |
| Alfum | 80@PAANa | 56 (160) {35} | 259 (91) {285} | 428 (77) {552} |
| Alfum | 80@PEG | 25 (89) {28} | 83 (32) {257} | 206 (54) {378} |
| Alfum | 80@PEI | 66 (176) {38} | 131 (45) {294} | 409 (76) {541} |
| Alfum | 80@PVA(98) | 43 (145) {30} | 300 (114) {262} | 444 (110) {405} |
| Alfum | 80@PVA(88)4 | 37 (123) {30} | 250 (95) {263} | 359 (87) {411} |
| Alfum | 80@PVP | 32 (83) {38} | 267 (94) {283} | 356 (74) {482} |
| | | $p \cdot p_0^{-1}$ = 0.05 | $p \cdot p_0^{-1}$ = 0.20 | $p \cdot p_0^{-1}$ = 0.90 |
| | MIL-160(Al) | 68 (-) {-} | 319 (-) {-} | 384 (-) {-} |
| MIL-160(Al) | 80@PAA | 73 (133) {55} | 319 (102) {260} | 389 (98) {396} |
| MIL-160(Al) | 80@PAANa | 93 (166) {56} | 264 (61) {268} | 295 (60) {491} |
| MIL-160(Al) | 80@PEG | 67 (123) {54} | 163 (49) {255} | 191 (60) {317} |
| MIL-160(Al) | 80@PEI | 41 (72) {57} | 125 (60) {271} | 382 (80) {480} |
| MIL-160(Al) | 80@PVA(98) | 58 (105) {55} | 163 (104) {258} | 346 (100) {344} |
| MIL-160(Al) | 80@PVA(88)4 | 64 (116) {55} | 269 (93) {258} | 328 (94) {350} |
| MIL-160(Al) | 80@PVP | 53 (91) {58} | 240 (103) {270} | 397 (94) {421} |
| | | $p \cdot p_0^{-1}$ = 0.40 | $p \cdot p_0^{-1}$ = 0.60 | $p \cdot p_0^{-1}$ = 0.90 |
| | MIL-101(Cr) | 122 (-) {-} | 1082 (-) {-} | 1142 (-) {-} |
| MIL-101(Cr) | 80@PAA | 206 (190) {108} | 791 (89) {890} | 847 (84) {1003} |
| MIL-101(Cr) | 80@PAANa | 403 (305) {132} | 660 (70) {948} | 712 (65) {1097} |
| MIL-101(Cr) | 80@PEG | 325 (330) {98} | 724 (84) {867} | 778 (84) {923} |
| MIL-101(Cr) | 80@PEI | 299 (206) {145} | 470 (50) {944} | 580 (53) {1086} |
| MIL-101(Cr) | 80@PVA(98) | 198 (190) {104} | 677 (77) {877} | 718 (76) {951} |
| MIL-101(Cr) | 80@PVA(88)4 | 251 (239) {105} | 759 (86) {880} | 805 (84) {956} |
| MIL-101(Cr) | 80@PVP | 397 (310) {128} | 791 (87) {911} | 853 (83) {1027} |

[a] Prepared by liquid nitrogen freeze-drying (LNFD).

[b] Calculated water uptake value as the sum of the mass-weighted uptake of the MOF and polymer at the respective relative pressure:

$$\text{Water uptake calc.} = \frac{\text{wt\% of polymer}}{100} \times (\text{water uptake polymer}) + \frac{\text{wt\% of MOF}}{100} \times (\text{water uptake MOF})$$

The value "water uptake polymer" (see Fig. 1) and "water uptake MOF" (see Fig. 6) can be taken from the adsorption isotherm of the MOF and polymer at the related relative pressure.

addition of hydrophilic groups derived from the polymer could be responsible for the hydrophilic shift. In the literature, it was shown that, a reduced pore size distribution in the range of 15 Å and 35 Å in micro- and mesoporous silica also causes a hydrophilic shift [68]. Using the pore size distribution derived from argon sorption, we also showed a pore size reduction in the range of 20–35 Å for MIL-101(Cr)@polymer monoliths. It is also reported that hydrophilic functional groups attached to the organic ligand can supply additional nucleation sites [12], which is provided in this work by the hydrophilic polymers. This slight difference in pore size distribution and the effect of functional groups of polymers could be the result of the synergistic effect for the observed hydrophilic shift.

### 3.10. Preparation of MOF@polymer monoliths via cryopolymerization

Cross-linking of the polymer was tested to investigate the influence to the monolith formation and its corresponding textural properties. We used the cross-linking of PVA with glutaraldehyde. However, the cross-linked CP-PVA allowed only for a low maximum loading of 45 wt% MOF and the resulting sorption properties were not competitive to the non-cross-linked monoliths. Hence, this method is covered only superficially here. The detailed results can be found in the Supp. Info.

The IR spectra of MOF@CP-polymer composites represent MOF and PVA without any additional or missing absorption bands (see Fig. S24 and Fig. S25 in Supp. Info.).

Well-defined macropores are visible in the SEM-image of MIL-101 (Cr)45@CP-PVA(88)3 monolith (Fig. 7).

Yet, only for the MIL-101(Cr)45@CP-PVA(98) monolith is the pore accessibility comparable with the monoliths obtained via freeze-casting (see Table S4, Supp. Info. for the uptake properties of the cross-linked and cryopolymerized composites). The apparent S(BET) of MIL-101(Cr) 45@CP-PVA(98) is 828 $m^2 g^{-1}$ representing 74% of the calculated value.

The apparent S(BET) of MIL-101(Cr)45@CP-PVA(88)2 and 3 are 137 and 133 $m^2\ g^{-1}$ indicating only 13% and 12% of the calculated value, respectively. Also, Alfum45@CP-PVA(98) showed a much lower nitrogen accessibility and with decreasing molecular weight of PVA the calculated apparent S(BET) decreased dramatically. However, the loss in water uptake capacity of the cryopolymerized composites is less dramatic. Most of the MIL-101(Cr)45 and Alfum45 composites still reach about 50% of the calculated water uptake (Fig. 8). Unfortunately, it was not possible to obtain a cross-linked monolith material with a larger fraction than 45 wt% of MOF by cryopolymerization. Raising the concentration of glutaraldehyde from 10 g $L^{-1}$ to 50 g $L^{-1}$ was not successful for the monolith preparation.

## 4. Conclusions

The freeze-casting method was successfully applied to form monoliths with the polymers PAA, PAANa, PEG, PEI, PVA(98), PVA(88) or PVP and the MOFs Alfum, MIL-160(Al) or MIL-101(Cr). In all monoliths the crystallinity of the MOFs was retained. For the first time, we achieved an almost negligible pore blocking of the embedded MOFs by applying the freeze-casting method in the preparation of the MOF@-polymer monoliths. Optimization experiments showed that freezing with liquid nitrogen (LN) and subsequent freeze-drying (LNFD) is the method of choice for a rapid monolith formation and its shaping together with retention of the porosity (BET surface and pore volume) of the MOFs. The molecular weight of the polymer affected the porosity properties of the monolith such that higher molecular weights induced less pore blocking of the MOFs in the monoliths.

For the MOFs Alfum and MIL-160(Al) the best porosity results concerning *S*(BET) and V(pore) in the monoliths were obtained with the polymers PVA and PVP. Concerning water loading with Alfum, the polymer monoliths provide highly satisfactory results from 87% to 114% of the calculated water loading at $p{\cdot}p_0^{-1} = 0.35$; except for the PEI and PEG composites. With MIL-160(Al)80@PAA, PVA(98), PVA(88)4 and PVP the water loading was about 100% of the calculated water loading at $p{\cdot}p_0^{-1} = 0.20$. In case of MIL-101(Cr), almost all of its polymer monoliths achieved over 85% of the calculated *S*(BET) and 90% of the calculated V(pore), PEI being the only exception with 47% of the calculated *S*(BET) and 52% of the calculated V(pore).

Another remarkable result is the hydrophilic shift in the MIL-101(Cr)@polymer composites compared to neat MIL-101(Cr) such that the hydrophilic polymers induce a water uptake at lower relative pressure ($p \cdot p_0^{-1}$) than what the more hydrophobic MIL-101(Cr) would show. This hydrophilic effect was also observed in Alfum@polymer and in MIL-160(Al)@polymer monoliths in the lower relative pressure region of $p{\cdot}p_0^{-1} \leq 0.15$ and $p{\cdot}p_0^{-1} \leq 0.05$, respectively.

Although the effect of molecular weight for freeze casting was negligible and showed only minor changes in the sorption properties, the effect of molecular weight plays a critical role in the monolith prepared by in-situ PVA cross-linking. Cross-linking of the PVA polymers did not lead to an improvement in the sorption properties of the composites.

We see great potential for the easy to use freeze-casting method to obtain stable polymer monolith composites with improved sorption properties for many other MOFs.

## Author Contribution Statement

EH performed the experiments, collected and interpreted the data and wrote and revised the manuscript.

SPH has carried out the cryopolymerization part in the manuscript.

BT did preliminary experiments and synthesized the MOF MIL-160.

CS obtained the SEM images and helped with the IR measurements.

CJ outlined the idea together with EH, provided feedback to the work, refined the manuscript.

## Declaration of competing interest

The authors declare that they have no known competing financial interests or personal relationships that could have appeared to influence the work reported in this paper.

## Acknowledgments

The authors gratefully acknowledge the financial support of the Federal German Ministry of Education and Research (BMBF) in the project Optimat under grant no. 03SF0492C. We thank Mr. Simon Millan for helpful discussions. We are indebted to Mrs. Birgit Tommes for measuring the IR spectra.

## Appendix A. Supplementary data

Supplementary data to this article can be found online at https://doi.org/10.1016/j.micromeso.2019.109907.

## References

[1] S.R. Batten, N.R. Champness, X.-M. Chen, J. Garcia-Martinez, S. Kitagawa, L. Öhrström, M. O'Keeffe, M.P. Suh, J. Reedijk, Pure Appl. Chem. 85 (2013) 1715–1724.
[2] P.Z. Moghadam, A. Li, S.B. Wiggin, A. Tao, A.G.P. Maloney, P.A. Wood, S.C. Ward, D. Fairen-Jimenez, Development of a Cambridge structural database subset: a collection of metal-organic frameworks for past, present, and future, Chem. Mater. 29 (2017) 2618–2625.
[3] J.Y. Lee, O.K. Farha, J. Roberts, K.A. Scheidt, S.B.T. Nguyena, J.T. Hupp, Chem. Soc. Rev. 38 (2009) 1450–1459.
[4] L. Jiao, Y. Wang, H.-L. Jiang, Q. Xu, Adv. Mater. 30 (1–23) (2018) 1703663.
[5] R.-B. Lin, S. Xiang, H. Xing, W. Zhou, B. Chen, Coord. Chem. Rev. 378 (2019) 87–103.
[6] J.-R. Li, J. Sculley, H.-C. Zhou, Chem. Rev. 112 (2012) 869–932.
[7] J.A. Mason, M. Veenstra, J.R. Long, Chem. Sci. 5 (2014) 32–51.
[8] S.K. Henninger, H.A. Habib, C. Janiak, J. Am. Chem. Soc. 131 (2009) 2776–2777.
[9] S.K. Henninger, S.-J. Ernst, L. Gordeeva, P. Bendix, D. Fröhlich, A.D. Grekova, L. Bonaccorsi, Y. Aristov, J. Jaenchen, Renew. Energy 110 (2017) 59–68.
[10] M.F. de Lange, B.J. van Velzen, C.P. Ottevanger, K.J.F.M. Verouden, L.C. Lin, T.J. H. Vlugt, J. Gascon, F. Kapteijn, Langmuir 31 (2015) 12783–12796.
[11] E. Hastürk, S.-J. Ernst, C. Janiak, Curr. Opin. Chem. Eng. 24 (2019) 26–36.
[12] M.F. de Lange, K.J.F.M. Verouden, T.J.H. Vlugt, J. Gascon, F. Kapteijn, Chem. Rev. 115 (2015) 12205–12250.
[13] H. Demir, M. Mobedi, S. Ülkü, Renew. Sustain. Energy Rev. 12 (2008) 2381–2403.
[14] S. Cui, M. Qin, A. Marandi, V. Steggles, S. Wang, X. Feng, F. Nouar, C. Serre, Sci. Rep. 8 (1–9) (2018) 15284.
[15] H. Kim, S. Yang, S.R. Rao, S. Narayanan, E.A. Kapustin, H. Furukawa, A.S. Umans, O.M. Yaghi, E.N. Wang, Science 356 (2017) 430–434.
[16] E. Leung, U. Müller, N. Trukhan, H. Mattenheimer, G. Cox, S. Blei, Process for Preparing Porous Metal-Organic Frameworks Based on Aluminum Fumarate, US 201/0082864 A1, 2012 Apr 5.
[17] A. Cadiau, J.S. Lee, D.D. Borges, P. Fabry, T. Devic, M.T. Wharmby, C. Martineau, D. Foucher, F.T. Taulelle, C.-H. Jun, Y.K. Hwang, N. Stock, M.F. De Lange, F. Kapteijn, J. Gascon, G. Maurin, J.-S. Chang, C. Serre, Adv. Mater. 27 (2015) 4775–4780.
[18] G. Férey, C. Mellot-Draznieks, C. Serre, F. Millange, J. Dutour, S. Surblé, I. Margiolaki, Science 309 (2005) 2040–2042.
[19] A. Permyakova, O. Skrylnyk, E. Courbon, M. Affram, S. Wang, U.-H. Lee, A. H. Valekar, F. Nouar, G. Mouchaham, T. Devic, G.D. Weireld, J.-S. Chang, N. Steunou, M. Frère, C. Serre, ChemSusChem 10 (2017) 1419–1426.
[20] F. Jeremias, D. Fröhlich, C. Janiak, S.K. Henninger, RSC Adv. 4 (2014) 24073–24082.
[21] P. Küsgens, M. Rose, I. Senkovska, H. Fröde, A. Henschel, S. Siegle, S. Kaskel, Microporous Mesoporous Mater. 120 (2009) 325–330.
[22] Y.I. Aristov, Appl. Therm. Eng. 50 (2013) 1610–1618.
[23] N. Ko, P.G. Choi, J. Hong, M. Yeo, S. Sung, K.E. Cordova, H.J. Park, J.K. Yang, J. Kim, J. Mater. Chem. 3 (2015) 2057–2064.
[24] G. Akiyama, R. Matsuda, H. Sato, A. Hori, M. Takata, S. Kitagawa, Microporous Mesoporous Mater. 157 (2012) 89–93.
[25] A. Khutia, H.U. Rammelberg, T. Schmidt, S.K. Henninger, C. Janiak, Chem. Mater. 25 (2013) 790–798.
[26] M. Wickenheisser, F. Jeremias, S.K. Henninger, C. Janiak, Inorg. Chim. Acta 407 (2013) 145–152.
[27] Z. Liu, Y. Chen, J. Sun, H. Lang, W. Gao, Y. Chi, Inorg. Chim. Acta 473 (2018) 29–36.
[28] U. Betke, M. Klausa, J.G. Eggebrecht, M. Scheffler, A. Lieb, Microporous Mesoporous Mater. 265 (2018) 43–56.
[29] M. Wickenheisser, T. Paul, C. Janiak, Microporous Mesoporous Mater. 220 (2016) 258–269.

[30] M. Wickenheisser, A. Herbst, R. Tannert, B. Milow, C. Janiak, Microporous Mesoporous Mater. 215 (2015) 143–153.
[31] M. Wickenheisser, C. Janiak, Microporous Mesoporous Mater. 204 (2015) 242–250.
[32] B. Valizadeh, T.N. Nguyen, K.C. Stylianou, Polyhedron 145 (2018) 1–15.
[33] M. Rubio-Martinez, C. Avci-Camur, A.W. Thornton, I. Imaz, D. Maspoch, M.R. Hill, Chem. Soc. Rev. 46 (2017) 3453–3480.
[34] P.B. Bendix, S.K. Henninger, H.-M. Henning, Ind. Eng. Chem. Res. 55 (2016) 4942–4947.
[35] P. Bendix, G. Füldner, M. Möllers, H. Kummer, L. Schnabe, S. Henninger, H.-M. Henning, Appl. Therm. Eng. 124 (2017) 83–90.
[36] L. Qian, H. Zhang, J. Chem. Technol. Biotechnol. 86 (2011) 172–184.
[37] A. Ahmed, T. Hasell, R. Clowes, P. Myers, A.I. Cooper, H. Zhang, Chem. Commun. 51 (2015) 1717–1720.
[38] L. Huber, P. Ruch, R. Hauert, S.K. Matam, G. Saucke, S. Yoon, Y. Zhange, M. M. Koebel, RSC Adv. 6 (2016) 80729–80738.
[39] L. Ma, A. Jin, Z. Xie, W. Lin, Angew. Chem. Int. Ed. 48 (2009) 9905–9908.
[40] Q. Fu, L. Wen, L. Zhang, X. Chen, D. Pun, A. Ahmed, Y. Yang, H. Zhang, ACS Appl. Mater. Interfaces 9 (2017) 33979–33988.
[41] H. Zhu, Q. Zhang, S. Zhu, Chem. Eur J. 22 (2016) 8751–8755.
[42] F.M. Plieva, I.Y. Galaev, W. Noppe, B. Mattiasson, Trends Microbiol. 16 (2008) 543–551.
[43] T.M.A. Henderson, K. Ladewig, D.N. Haylock, K.M. McLean, A.J. O'Connor, J. Mater. Chem. B 1 (2013) 2682–2695.
[44] N. Sahiner, S. Demirci, J. Appl. Polym. Sci. 133 (1–13) (2016) 43478.
[45] Y. Lin, Q. Yan, C. Kong, L. Chen, Sci. Rep. 3 (1–7) (2013) 1859.
[46] P. Li, S. Zhang, S. Chen, Q. Zhang, J. Pan, B. Ge, J. Appl. Polym. Sci. 108 (2008) 3851–3858.
[47] M. Thommes, K. Kaneko, A.V. Neimark, J.P. Olivier, F. Rodriguez-Reinoso, J. Rouquerol, K.S. Sing, Pure Appl. Chem. 87 (2015) 1051–1069.
[48] J. Rouquerol, P. Llewellyn, F. Rouquerol, Stud. Surf. Sci. Catal. 160 (2007) 49–56.
[49] T. Zhao, F. Jeremias, I. Boldog, B. Nguyen, S.K. Henninger, C. Janiak, Dalton Trans. 44 (2015) 16791–16801.
[50] J. Yang, Q. Zhao, J. Li, J. Dong, Microporous Mesoporous Mater. 130 (2010) 174–179.
[51] F.M. Plieva, M. Karlsson, M.-R. Aguilar, D. Gomez, S. Mikhalovsky, I.Y. Galaev, B. Mattiasson, J. Appl. Polym. Sci. 100 (2006) 1057–1066.
[52] E. Leung, U. Muller, N. Trukhan, H. Mattenheimer, G. Cox, S. Blei, Process for preparing porous metal organic frameworks based on Aluminum fumarate. US patent (05.04.12.) 2012/0082864A1.
[53] M. Bakass, J.P. Bellat, A. Mokhlisse, G. Bertrand, J. Appl. Polym. Sci. 100 (2006) 1450–1456.
[54] J.A. Baird, R. Olayo-Valles, C. Rinaldi, L.S. Taylor, J. Pharm. Sci. 99 (2010) 154–168.
[55] H.M.L. Thijs, C.R. Becer, C. Guerrero-Sanchez, D. Fournier, R. Hoogenbooma, U. S. Schubert, J. Mater. Chem. 17 (2007) 4864–4871.
[56] E. Marin, J. Rojas, Int. J. Pharm. Sci. Rev. Res. 30 (2015) 189–194.
[57] J. Teng, S. Bates, D.A. Engers, K. Leach, P. Schields, Y. Yang, J. Pharm. Sci. 99 (2010) 3815–3825.
[58] M.F. Daniel, B. Desbat, F. Cruege, O. Trinquet, J.C. Lassegues, Solid State Ion. 28–30 (1988) 637–641.
[59] T. Hashida, K. Tashiro, S. Aoshima, Y. Inaki, Macromolecules 35 (2002) 4330–4336.
[60] E. Riedel, C. Janiak, Anorganische Chemie, Walter de Gruyter, 2015, p. 347.
[61] N. Mehio, S. Dai, D. Jiang, J. Phys. Chem. A 118 (2014) 1150–1154.
[62] J. Möllmer, E.B. Celer, R. Luebke, A.J. Cairns, R. Staudt, M. Eddaoudi, M. Thommes, Microporous Mesoporous Mater. 129 (2010) 345–353.
[63] A. Nuhnen, D. Dietrich, S. Millan, C. Janiak, ACS Appl. Mater. Interfaces 10 (2018) 33589–33600.
[64] M. Zhou, P.R. Nemade, X. Lu, X. Zeng, E.S. Hatakeyama, R.D. Noble, D.L. Gin, J. Am. Chem. Soc. 129 (2007) 9574–9575.
[65] M. Wahiduzzaman, D. Lenzen, G. Maurin, N. Stock, M.T. Wharmby, Eur. J. Inorg. Chem. (2018) 3626–3632.
[66] D. Lenzen, J. Zhao, S.-J. Ernst, M. Wahiduzzaman, A.K. Inge, D. Fröhlich, H. Xu, H.-J. Bart, C. Janiak, S. Henninger, G. Maurin, X. Zou, N. Stock, Nat. Commun. 10 (2019) 3025.
[67] S. Gökpinar, S.-J. Ernst, E. Hastürk, M. Möllers, I. El Aita, R. Wiedey, N. Tannert, S. Nießing, S. Abdpour, A. Schmitz, J. Quodbach, G. Füldner, S.K. Henninger, C. Janiak, Ind. Eng. Chem. Res. 58 (2019) 21493–21503, https://doi.org/10.1021/acs.iecr.9b04394.
[68] S. Saliba, P. Ruch, W. Volksen, T.P. Magbitang, G. Dubois, B. Michel, Microporous Mesoporous Mater. 226 (2016) 221–228.